IEEE Access
Multidisciplinary ⋮ Rapid Review ⋮ Open Access Journal

Received November 5, 2019, accepted November 27, 2019, date of publication December 10, 2019,
date of current version December 27, 2019.

Digital Object Identifier 10.1109/ACCESS.2019.2958633

Effect of Incident Area Size on Estimation of EMI Shielding Effectiveness for Ultra-High Performance Concrete With Carbon Nanotubes

MYUNGJUN JUNG[1], YOUNG-SOON LEE[2], AND SUNG-GUL HONG[1]
[1]Department of Architect and Architectural Engineering, Seoul National University, Seoul 08826, South Korea
[2]Department of Electronic Engineering, Kumoh National Institute of Technology, Gumi 39177, South Korea

Corresponding author: Sung-Gul Hong (sglhong@snu.ac.kr)

ABSTRACT The electromagnetic interference (EMI) shielding effectiveness (SE) of Ultra-High Performance Concrete (UHPC) mixed with carbon nanotubes (CNTs) (UHPC/CNT composites) having a thickness of 200 mm in the frequency range of 10 kHz to 18 GHz was investigated according to IEEE-STD-299 for the first time. In addition, the effect of the size of the incident area on the SE was analyzed by comparing the SE results for two different incident areas: a small incident area of 300 × 300 mm^2 and a large incident area of 1200 × 1200 mm^2. A significant improvement in the SE of the UHPC/CNT composite was achieved by increasing the CNT content up to the percolation threshold. Experimental observations indicated that the small incident area caused a distortion of the SE in the magnetic field owing to the aperture effect, whereas it had little effect on the SE for a plane wave. Thus, to eliminate the effect of the aperture on the measurement of the SE for UHPC/CNT composites in a magnetic field, an incident area larger than 1200 × 1200 mm^2 is recommended. According to a statistical analysis of the experimental results, a practical model was proposed to estimate the SE of cementitious material for different frequency ranges.

INDEX TERMS Carbon nanotube (CNT), electromagnetic interference (EMI), IEEE-STD-299, shielding effectiveness (SE), ultra-high performance concrete (UHPC).

I. INTRODUCTION

Electromagnetic interference (EMI) shielding mainly results from reflection on the surface and/or absorption of EM waves by means of a conductive material [1]. In the construction field, the importance of EMI shielding is increasing with the rapid growth of radio communication and the ubiquity of electronic devices because EM waves can directly affect the human body and induce the growth of tumors [2]–[4]. In addition, it can cause the malfunction of electronic devices or paralyze security facilities associated with finance data, power plant control, and defense information sectors, etc. Hence, EMI shielding is not an option but a necessity in such areas.

Concrete, as a basic building construction material, cannot be used for EMI shielding owing to its high electrical resistivity in the range of 10^6–$10^9\,\Omega\cdot$m [5]. However, carbon materials such as carbon nanotubes (CNTs), graphene, and carbon black are considered to be effective conductive fillers owing to their extraordinary electrical conductivity (> 1000 times higher than that of copper) [6]. Thus, numerous studies on the application of carbon materials in the development of conductive cementitious materials with high shielding effectiveness (SE) have been reported over the last few decades [7]–[12]. However, most previous studies were based on ordinary cement paste or mortar, and it is difficult to extend their results directly to Ultra-High Performance Concrete (UHPC), which exhibits completely different mechanical properties, including excellent durability and crack resistance with a compressive strength of > 150 MPa owing to the dense packing of particles with a low water-to-cement ratio (w/c). Therefore, it is necessary to investigate the SE of UHPC with carbon materials.

There are several standard test methods for measuring EMI SE, such as ASTM D4935-18, ASTM E1851-15,

The associate editor coordinating the review of this manuscript and approving it for publication was Chaitanya U. Kshirsagar.

MIL-STD-188-125-1, and IEEE-STD-299 [13]–[16]. These methods can be classified into small-sample testing and large-sample testing according to the required geometry of the sample. ASTM D4935-18 can be regarded as being representative of small-sample testing, and the other methods can be considered to be large-sample testing. Most previous studies were based on small-sample testing methods because the samples are easy to fabricate and simple to test, reducing the required amount of labor, resources, etc. However, this method is not appropriate for cementitious material [12] because it is impossible to fabricate samples as thin as 25 μm, which is the required dimension according to ASTM D4935-18. In addition, if the thickness of the sample is up to several millimeters, the SE can be overestimated via leaking of the signal through the gap between the coaxial transverse EM-cell. Moreover, it is difficult to represent the SE measured by small-sample testing as that of an actual structure. Thus, this method should only be used to roughly estimate the effect of different components on the SE of cementitious material.

IEEE-STD-299 is a representative large-sample testing method that can indicate the SE of an actual structure. This method requires that the incident area of the sample should be equal to or greater than 2.0 × 2.0 m^2. However, it is difficult to fabricate test samples satisfying the required dimensions. Nevertheless, there is no previous research that has been performed to determine the requirement of the incident area size and the effect of the small size of the incident area on the EMI SE.

Hence, in this study, the EMI SE of UHPC with CNTs (UHPC/CNT composites) having a thickness of 200 mm in the frequency range of 10 kHz to 18 GHz was investigated according to IEEE-STD-299 for the first time. In addition, the effect of the size of the incident area on the SE was examined using testing samples with two different incident areas. Finally, a practical model for estimating the SE was developed by analyzing the experimental data using statistical analyses.

II. EXPERIMENTAL PROGRAM

A. MATERIAL AND MIX PROPORTION

Test samples were fabricated using identical materials: multi wall CNTs (MWCNTs) made by Kumho Inc., Type I Portland cement (Union Cement Co., Ltd.), silica fume (Grade 940U, Elkem), silica powder (S-SIL 10, SAC) and silica sand. MWCNTs produced via chemical vapor deposition were used. The properties of the MWCNTs are listed in Table 1.

The mix proportion is listed in Table 2. Six different contents of CNTs (0, 0.2, 0.5, 0.8, 1.0 and 2.0 by weight percent of cement) were mixed with the reference UHPC mixture. The weight ratios of water and super plasticizer (SPPL) were kept constant at 0.23 and 0.04, respectively, with respect to the weight of the cement. In the case of sample CNT2.0, a w/c of 0.28 was used by adding extra water so that the flow was equal to that of sample CNT1.0 to prevent false setting due to the rapid decrease of the flow for the UHPC with a high CNT dosage.

TABLE 1. Properties of CNTs.

Avg. diameter (nm)	Density (g/m^3)	Length (μm)	Purity (wt.%)	Specific surface area (m^2/g)
10–20	100,000–150,000	10–70	> 95	165–205

B. TEST SAMPLE PREPARATION

The test sample preparation consists of four steps: (a) fabrication of the dispersed CNT solution; (b) mixing of the dry pre-mixture with the solution; (c) sample casting; and (d) curing.

Sonication is a widely used method, and was performed using an ultrasonic processor (VCX 750, Sonics Inc.) with a 25 mm cylindrical boost probe to fabricate a dispersed CNT solution. Certain amounts of distilled water and SPPL were added to a jacketed stainless steel beaker with CNTs. Then, the sonicator was operated at an amplitude of 80 % so as to deliver an energy of 35000–36000 J/min. The temperature of the beaker was kept at 7 °C using a chiller to prevent overheating of the sonicator. The sonication was continued until the average particle size of the CNTs was approximately 20–30 μm, as indicated by particle size analysis. In fact, it is difficult to disperse CNTs within the aqueous solution and the cement composite owing to its hydrophobic nature, high aspect ratio, and strong Van der Waals forces.

Once the dispersed CNT solution was prepared, UHPC dry pre-mixture was added to the dispersed CNT solution, and it was mixed for 5 min using a Hobart mixer. Thereafter, fresh mixtures were decanted to molds.

Cubic test samples with volumes of 50 × 50 × 50 mm^3 were prepared to measure the electrical resistivity. Copper plates of volume 20 × 20 × 0.4 mm^3 were anchored into the samples as electrodes. The contact area of the copper plate with the composites was coated with silver paste to minimize the increase in the surface resistivity [17]–[21] and to prevent corrosion of the electrode during the curing. The samples for SE testing were fabricated in the form of two different square panels with a thickness of 200 mm, which is a typical building wall depth. The samples had different areas: 350 × 350 mm^2 and 1250 × 1250 mm^2, respectively. The incident areas of these test samples were smaller owing to the test settings: 300 × 300 mm^2 and 1200 × 1200 mm^2, respectively. The geometries of the test samples are presented in Fig. 1.

Fresh mixtures were cured for 24 h at room temperature. Then, the hardened samples were demolded and steam cured at 90 °C for 48 h. Thereafter, the samples were kept at 20 °C for 25 d so that the total curing period was 28 d. For electrical resistivity testing and SE testing, the moisture in the samples (which influenced the ionic conduction) was completely evaporated via oven drying at 60 °C for 2 d prior to testing in order to investigate the effect of the electronic conduction by the CNTs on the properties of the composite.

TABLE 2. Mix proportion (weight ratio of cement).

Sample	Cement	CNT	Silica fume	Silica powder	Silica sand	Super-plasticizer (SPPL)	Water/cement (w/c)
CNT0.0	1	0	0.25	0.35	1.1	0.04	0.23
CNT0.2		0.002					
CNT0.5		0.005					
CNT0.8		0.008					
CNT1.0		0.01					
CNT2.0		0.02					0.28

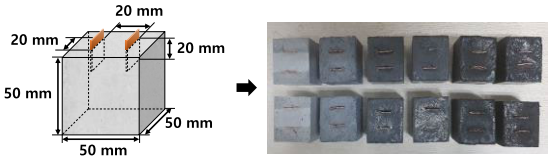

(a) Example of sample used for Electrical resistivity testing

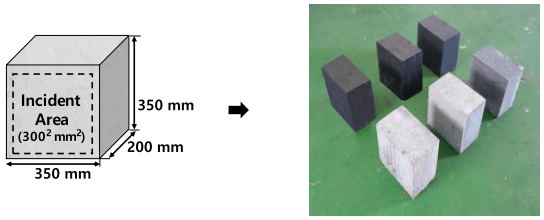

(b) Example of sample with a small incident area used for SE testing

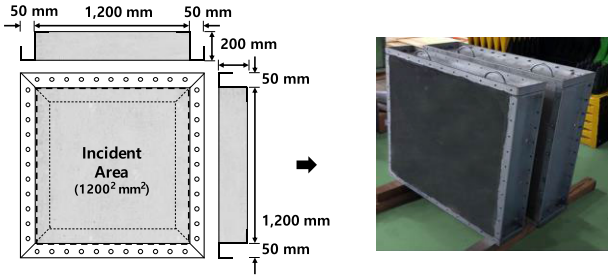

(c) Example of sample with a large incident area used for SE testing

FIGURE 1. Geometry of the test samples.

C. TEST METHOD

1) MORPHOLOGY OF DISPERSED CNTS

The degree of dispersion of the CNTs was evaluated by examining their morphology using microscopic and scanning electron microscopy (SEM) analyses with a light microscope (DM1750M, Leica) and a field-emission scanning electron microscope (FE SEM) (JSM-6700, JEOL Ltd.), respectively.

2) MEASUREMENT OF ELECTRICAL RESISTIVITY

The electrical resistance of the sample was measured via the four-wire method using an LCR meter (GW INSTEK LCR-6100). Six samples for each mix proportion were tested at a frequency of 10 kHz, and the average value of four samples except for the largest and smallest values was taken to be the representative electrical resistance. The electrical resistivity, i.e., the reciprocal of the electrical conductivity, was then calculated as follows:

$$\rho\,(\Omega \cdot m) = \frac{1}{\sigma} = R\frac{a}{L}, \tag{1}$$

where ρ is the electrical resistivity (Ω·m), σ is the electrical conductivity (S/m), R is the electrical resistance (Ω), a is the cross-sectional area of the composite between the electrodes (m^2), and L is the distance between the electrodes (m) [22].

3) EMI SE TEST BASED ON IEEE-STD-299

The EMI SE test according to IEEE-STD-299 was performed in the frequency range of 10 kHz–18 GHz [16]. Ten frequencies (i.e., 10 kHz, 100 kHz, 1 MHz, 10 MHz, 100 MHz, 1 GHz, 5 GHz, 10 GHz, 15 GHz, and 18 GHz) were selected as the frequencies of interest. A shielded chamber with dimensions 2400 × 2400 × 2400 mm^3 and an aperture made of steel and zinc, a spectrum analyzer (8563E, HP), a signal generator (SMB100A, ROHDE&SCHWARZ), and antenna kits were instrumented in the testing process.

Fig. 2 shows the details of the procedure for the EMI SE test. It starts with a free-space calibration (Fig. 2a). The values from the calibration (P_i) were taken as the zero point to be set on the receiver showing the difference readout from the nominal value. After the calibration was completed, a test sample was mounted on the aperture (Fig. 2b). Conductive gaskets were affixed to the gap between the chamber and the edge of the sample to prevent the leaking of EM waves. Then, the transmitting antenna was set up outside the chamber and the receiving antenna was placed inside the chamber. Both antennas were installed perpendicular to the geometric center of the sample (Fig. 2c). The distances between the antennas and the sample are listed in Table 3. Once the experimental setup was completed, a signal was generated at a particular frequency, and it was transmitted using the transmitting antenna. Then, the power level of the signal detected by the receiving antenna (P_t) passing through the sample was measured using a spectrum analyzer (Fig. 2d). Subsequently, the SE was calculated in terms of the ratio of EM power, as follows:

$$\text{SE (dB)} = 10\,\log\left(\frac{P_i}{P_t}\right), \tag{2}$$

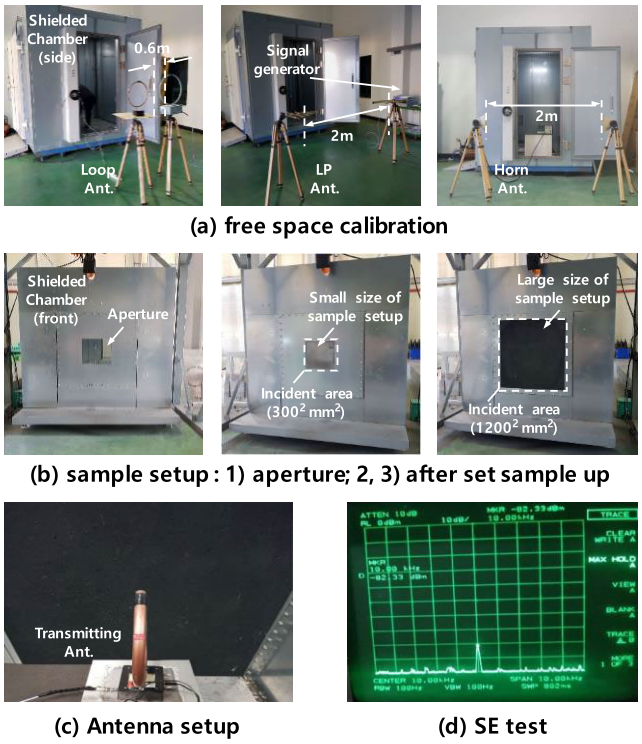

FIGURE 2. Procedure for the EMI SE test.

TABLE 3. Distance between Antennas and from sample.

Antenna type			Loop	Others
Distance (m)	Calibration (between antennas)		0.6	2
	Test (from sample)	Transmitting	0.3	1.7
		Receiving	0.3	0.3

where P_i and P_t represent the EM power measured in free space and from the sample, respectively.

To measure the SE, loop antennas were used in the low-frequency range (10 kHz–10 MHz), and bi-conical antennas were used in the resonant and transition range (10–100 MHz).

In the high-frequency range (100 MHz–18 GHz), log periodic (LP) antennas were used between 100 MHz and 1 GHz, and horn antennas were used in the range of 1–18 GHz.

The SE test was performed three times for each sample at each frequency of interest, and the average value was taken as a representative SE of the UHPC/CNT composites.

III. RESULTS AND DISCUSSION

A. DEGREE OF CNT DISPERSION

Fig. 3 shows the morphology of the CNTs in the solution state and their status after being embedded in the matrix. According to the microscopic analysis, the CNTs were further dispersed as the sonication progressed (Fig. 3a). In addition, the SEM images show that the morphology of the CNTs dispersed in the UHPC matrix was affected by the sonication process (Fig. 3b). The CNTs were generally anchored as single fibers with a size in the range of 1–10 μm, and few

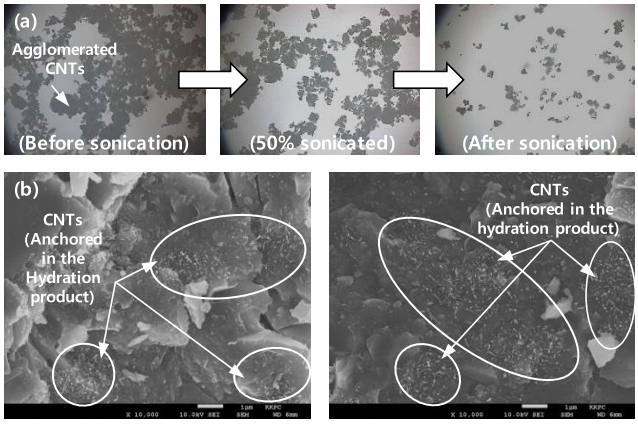

FIGURE 3. Morphology of the CNTs: (a) in solution status during the sonication; (b) embedded in the UHPC matrix (after 28 d of curing).

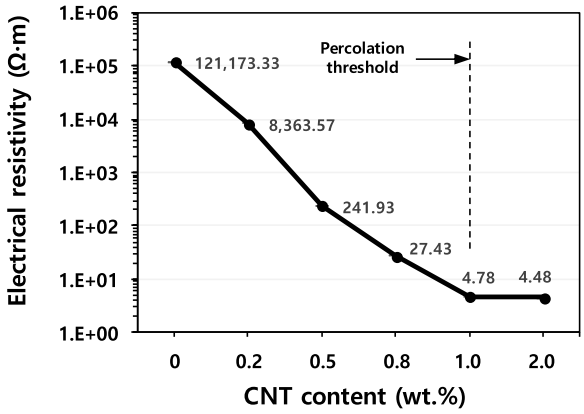

FIGURE 4. Electrical resistivity of the UHPC/CNT composites.

agglomerates were observed. Thus, the dispersion method used in this study is effective for dispersing CNTs within an aqueous solution and a UHPC matrix.

B. ELECTRICAL RESISTIVITY

Fig. 4 shows the electrical resistivity of the UHPC/CNT composites with respect to the CNT content. The electrical resistivity decreased significantly with an increase in the CNT content up to 1.0 wt.%. The obtained electrical resistivity at the CNT content of 0 wt.% (reference sample) was 121173.33 Ω·m. It was significantly reduced to 4.78 Ω·m with 1.0 wt.% CNTs. This indicates that the CNTs were uniformly distributed in the composites via the dispersion method [23]. If the dispersion of CNTs is poor, it is expected that the slope of the resistivity will be gradually inclined. However, an increase in the CNT content beyond 1.0 wt.% did not significantly reduce the electrical resistivity; the resistivity of the sample CNT2.0 was only 4.48 Ω·m even though it contained twice as many CNTs as CNT1.0. This is due to the percolation threshold, which is the ratio at which the conductive pathway is obtained owing to contact with adjacent conductive fibers [24]. A schematic diagram for the percolation threshold is shown in Fig. 5. The electrical resistivity of the UHPC/CNT composites decreased with

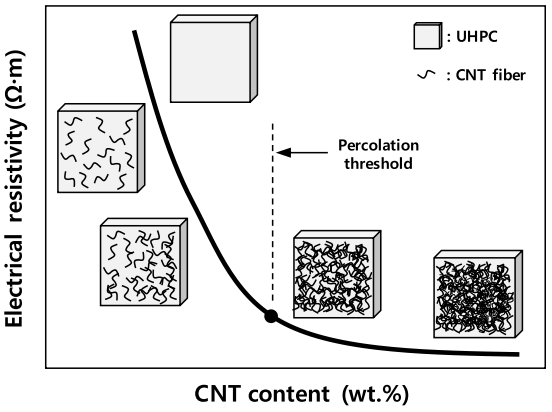

FIGURE 5. Schematic variation of electrical resistivity of the UHPC/CNT composites with respect to CNT content.

TABLE 4. Notations for EMI SE properties.

Notation	Quantity	Unit	Remark
K	impedance ratio		
c	velocity of light	m/s	3.0×10^8
f	frequency	Hz	
l	maximum dimension of aperture	m	
r	distance from antenna to sample	m	
t	thickness of sample	m	
ε_o	space permittivity	F/m	8.85×10^{-12}
ε_r	relative permittivity		
μ_o	space permeability	H/m	4.0×10^{-7}
μ_r	relative permeability		
λ	wavelength (c/f)	m	
σ_o	conductivity of copper	S/m	5.82×10^7
σ_r	relative conductivity		
δ	skin depth	m	

increasing dispersed CNT fibers uniformly distributed in the matrix; eventually, the CNT fibers constructed the conductive pathway by completely connecting adjacent fibers at the percolation threshold. Thus, increasing the CNT content beyond the percolation threshold did not significantly reduce the electrical resistivity because the conductive pathway was already constructed at the percolation threshold. Therefore, in this study, the CNT content of 1.0 wt.% can be regarded as the percolation threshold.

C. EMI SE CHARACTERISTICS

Table 4 presents the notations for the properties of EMI SE used in the following discussion.

1) BASICS OF SE THEORY

According to the law of the conservation of energy, in the process whereby incident energy passes through a material, a fraction of the energy is reflected by the surface of the material, absorbed inside, and reflected again on the opposite surface of the material. Hence, the SE developed while the EM waves pass through the material is theoretically the sum of the absorption loss (A), reflection loss (R), and multiple reflection loss (M). Thus, (2) can be expressed as follows:

$$\mathrm{SE\ (dB)} = A + R + M, \tag{3}$$

where R occurs owing to the impedance mismatch between the wave impedance (Z_w) and the intrinsic impedance of the material (Z_m). Z_w is well-defined in the near field and for plane waves (far field) at a distance (r) from the source, and is normalized by $\lambda/2\pi$. The near field can be classified into the electric field (E-field) and magnetic field (H-field). Thus, R should be considered separately according to the characteristics of Z_w for each field. Given that the SE of the E-field is always higher than that of the H-field, it is not mentioned in general. Therefore, the SE associated with the E-field is not discussed in this study. The impedance of each corresponding frequency region can be calculated as follows:

$$Z_w\ [\Omega] = k\sqrt{\frac{\mu_o}{\varepsilon_o}} \cong 120\,\pi k, \tag{4}$$

$$\text{where } k = \begin{cases} \dfrac{2\pi r}{\lambda} & \text{for H-field} \\ 1 & \text{for plane wave} \end{cases}$$

$$Z_m\ [\Omega] = \sqrt{\frac{\mu_o}{\varepsilon_o \varepsilon_r}} \quad \text{for dielectric.} \tag{5}$$

M in (3) can be neglected when A is more than 10 dB or in the case of a relatively thick material [25], [26]. In addition, similar to most cementitious materials, UHPC is a dielectric that experiences very little loss compared to metals. Hence, M can be ignored. A and R can be calculated using the following equations corresponding to the frequency region [25]:

$$A = 8.689\left(\frac{t}{\delta}\right) = 131.4t\sqrt{f\mu_r\sigma_r}, \tag{6}$$

$$R = \begin{cases} 20\log\dfrac{(1+K)^2}{4K} & \text{In general,} \quad (7a) \\ 14.6 - 10\log\left(\dfrac{\mu_r}{fr^2\sigma_r}\right) & \text{for H-field } (R_H), \quad (7b) \\ 168 - 10\log\left(\dfrac{f\mu_r}{\sigma_r}\right) & \text{for plane wave } (R_P). \quad (7c) \end{cases}$$

The preceding equations are valid for solid material (e.g., metal) without an aperture. In the opposite case (i.e., solid material with an aperture), the following equation (which describes the "aperture effect, S") should be considered to calculate the SE according to the theory of slot antennas [27].

$$S\ (\mathrm{dB}) = 20\log\left(\frac{\lambda}{2l}\right) = 20\log\left(\frac{c}{2fl}\right). \tag{8}$$

Equation (8) can be used only when the maximum dimension of the aperture (l) is less than half of the wavelength ($\lambda/2$).

2) ANALYSIS OF EMI SE TEST RESULTS

The EMI SE test results obtained for the samples with two different incident area sizes (i.e., a small incident area

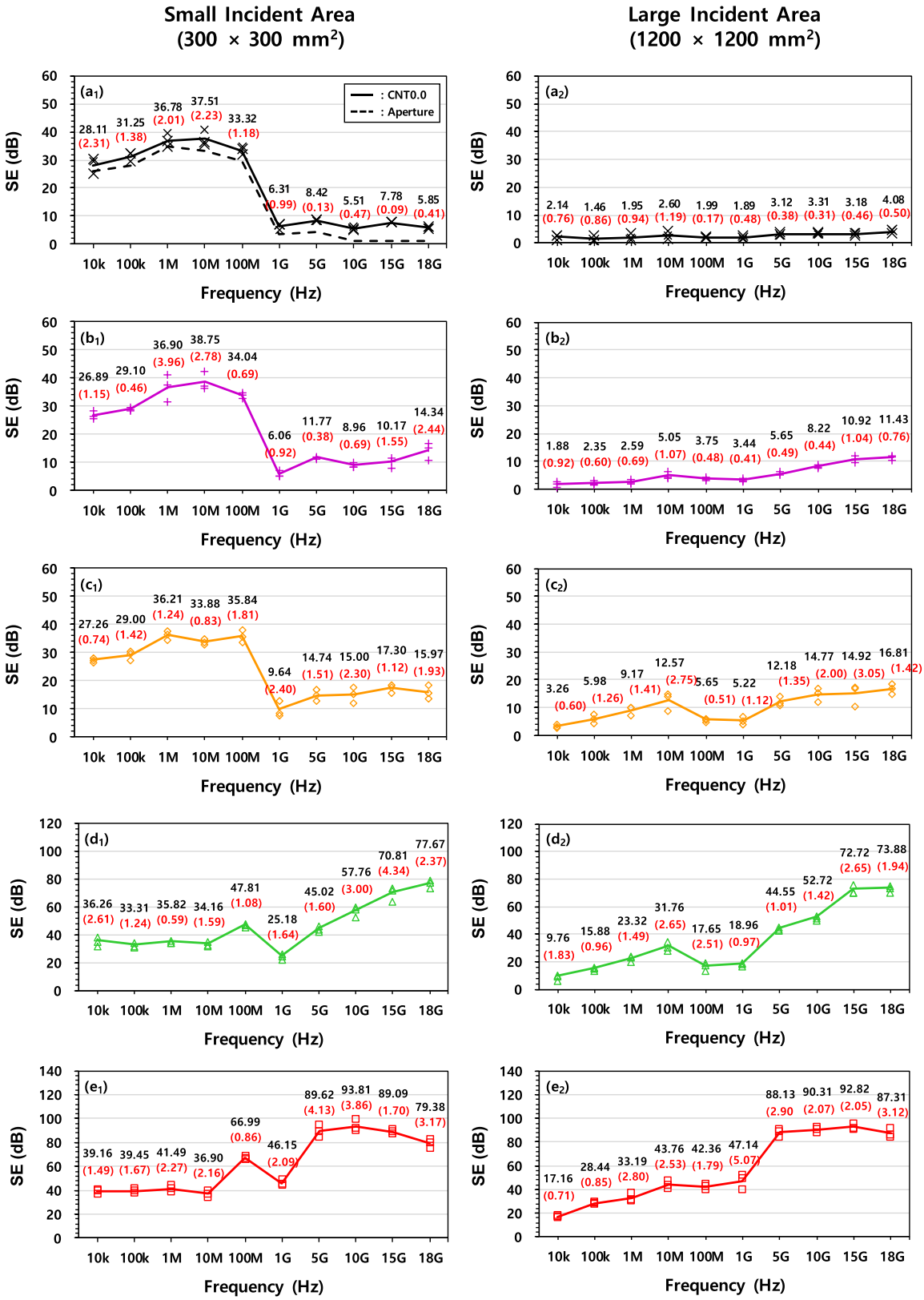

FIGURE 6. EMI SE test results for UHPC/CNT composites with different sizes of the incident area: (a) CNT0.0, (b) CNT0.2, (c) CNT0.5, (d) CNT0.8, (e) CNT1.0, (f) CNT2.0, and (g) average values for all samples (Symbols and lines represent the experimental values and average values, respectively. Black numbers and red numbers in parentheses above symbols represent the average values and standard deviations, respectively.)

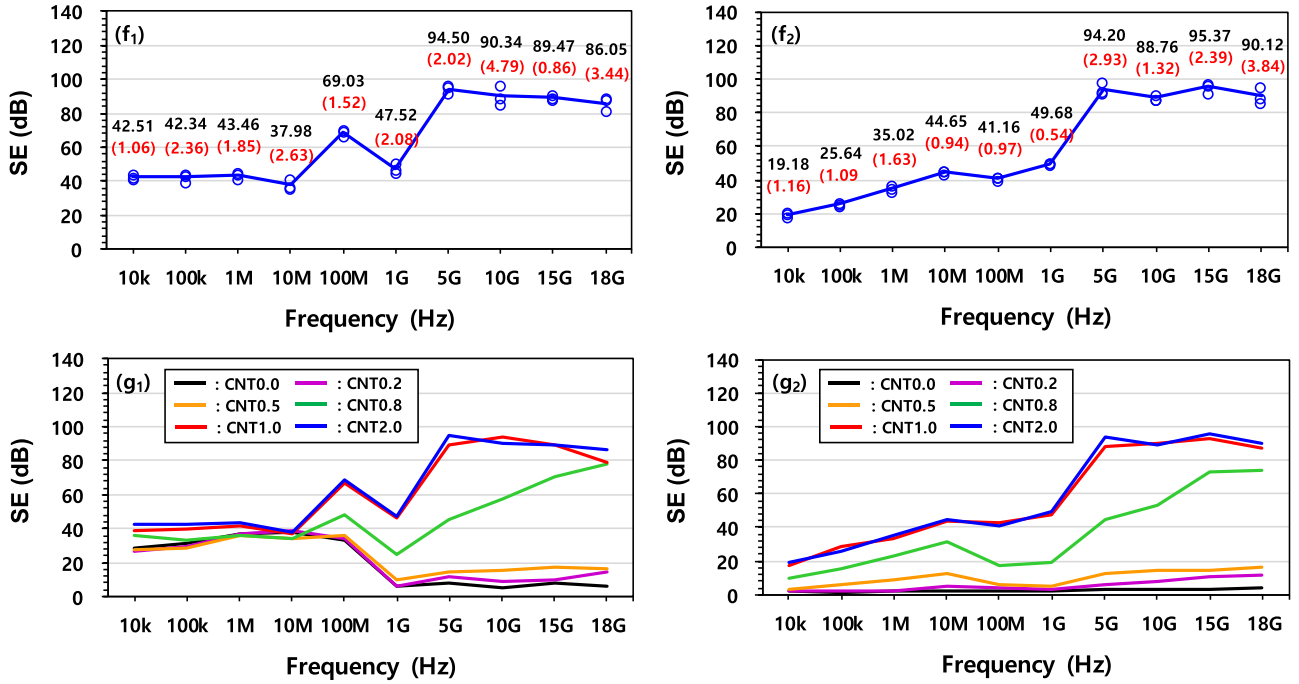

FIGURE 6. *(Continued.)* **EMI SE test results for UHPC/CNT composites with different sizes of the incident area: (a) CNT0.0, (b) CNT0.2, (c) CNT0.5, (d) CNT0.8, (e) CNT1.0, (f) CNT2.0, and (g) average values for all samples (Symbols and lines represent the experimental values and average values, respectively. Black numbers and red numbers in parentheses above symbols represent the average values and standard deviations, respectively.)**

of 300 × 300 mm^2 and a large incident area of 1200 × 1200 mm^2) are presented in Fig. 6 with respect to the CNT content. The standard deviation of the results for each sample was less than 5 dB, indicating that the test was performed appropriately, and the results can be regarded as reliable and repeatable. For all the samples, the SE improved as the CNT content increased in all frequency bands regardless of the size of the incident area. In addition, the SE was similar between samples CNT1.0 and CNT2.0 for the entire measured frequency range because there was little difference between their electrical resistivity values. This demonstrates that electrical resistivity is a major factor affecting the SE, and that there is a direct correlation between them.

One interesting observation from the experimental results was that the SE could be overestimated when a small sample with a relatively small incident area was used, owing to additional reflection loss (R_A). The SE obtained for small and large incident areas were almost identical at frequencies above 1 GHz. Meanwhile, in the case of the small incident area (Fig. 6a$_1$–g$_1$), the SE measured at frequencies below 1 GHz was more than twice that of the sample with large incident areas (Fig. 6a$_2$–g$_2$), although the samples were fabricated with the same batch mixtures and curing conditions. In particular, the reference sample (i.e., CNT0.0) had an SE value of 28.11 dB at 10 kHz, which appears to be a very high value considering that it has a high electrical resistivity. This was possibly due to R_A in a region of the shielded chamber in the vicinity of the aperture owing to the small size of the aperture (Fig. 7). Specifically, given that the transmitted λ was larger than the electrical dimension

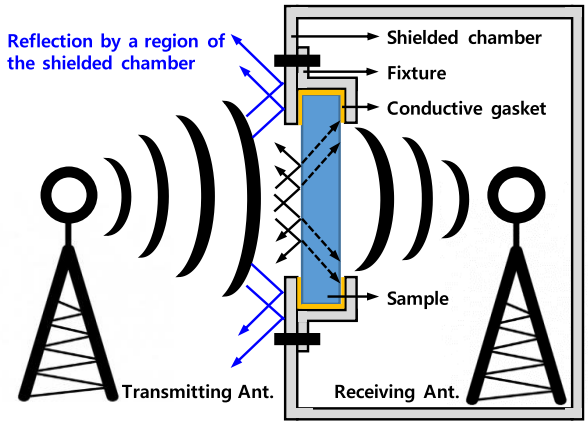

FIGURE 7. **Additional reflection loss (R_A) due to a region of the shielded chamber.**

of the aperture, which had a size equal to that of the small incident area, the transmitted EM waves were not completely incident on the sample. Thus, a portion of the waves was reflected by a region of the chamber. To validate this assumption (i.e., to examine the SE caused only by the aperture), the SE of the aperture was determined without mounting a sample. According to the results presented in Fig. 6a$_1$, the SE measured only with an aperture (black dotted line) was nearly equal to that of the reference sample below 1 GHz, whereas it was close to 0 dB at above 1 GHz. This means that as the transmitted λ decreased with an increase in the frequency up to 1 GHz, R_A decreased, and eventually, it disappeared at above 1 GHz because the value of λ became so

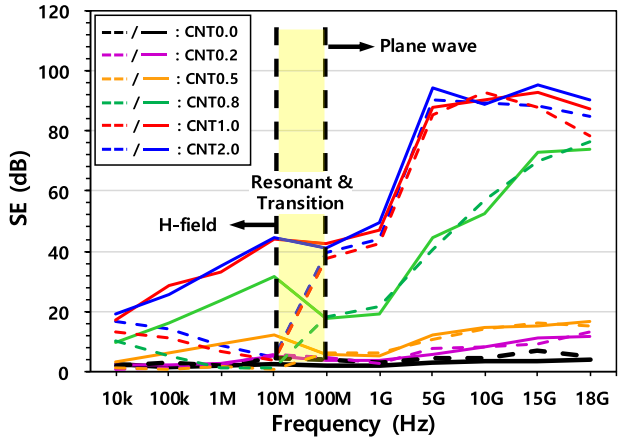

FIGURE 8. EMI SE results with additional reflection loss (R_A) eliminated (dotted and solid lines represent the results for the 300 × 300 mm^2 and 1200 × 1200 mm^2 incident areas, respectively).

small that the incoming waves were completely incident on the sample regardless of the aperture dimension. Therefore, to evaluate the SE of UHPC/CNT composites, it is more effective to subtract the SE of the aperture from the SE measured by the conventional method (i.e., IEEE-STD-299) to eliminate the contribution of R_A. By applying this approach, the SE test results (Fig. 6g) are represented in Fig. 8 (i.e., the SE of the aperture was subtracted from the SE test results). The reference sample exhibited low SE values close to 0 dB for all frequency bands regardless of the size of the incident area. In addition, the SE of the samples containing CNTs for the small incident area at 10 kHz was reduced to values that are similar to those for the large incident area. These results validate the assumption that the SE can be overestimated if it is tested using a sample with a relatively small incident area.

Another observation is that a small incident area can result in a distorted SE in the H-field owing to the aperture effect, whereas it has little effect for a plane wave. With an increase in the frequency in the range of 10 kHz–10 MHz, the SE of the samples with a small incident area decreased, whereas that of the large incident area samples increased. This was also because of the size of the aperture. The experimental frequency ranges can be classified into three regions—the H-field (below 10 MHz), resonant and transition region (from 10 MHz to 100 MHz), and plane wave (above 100 MHz)—according to the SE theory and the experimental setting (e.g., distances from the transmitting antenna to the sample). In the H-field, both A and R of the solid material without an aperture increases with increasing frequency, as indicated by (6) and (7b). However, the UHPC, which is similar to most cementitious materials, is porous with multiple size pores ranging from the nanometers to millimeters [28]. The pores in the material can be regarded as micro-apertures that can cause shield discontinuity. Thus, it can be assumed that in the case of the UHPC/CNT composites, the UHPC matrix with CNTs acted as a shield, and the pores played the role of apertures. Therefore, (8) allows the SE of a material with an aperture (i.e., corresponding to the effect of pores on the SE) to be considered in addition to the equations for the SE of materials without an aperture (i.e., corresponding to the effect of the UHPC matrix with CNTs on the SE). In the H-field, given that the contribution of A is negligibly small and R is the dominant factor, the new R_H (R_H^*) in which the aperture effect is considered can be expressed in the following form as the sum of (7b) and (8):

$$R_H^*(\text{dB}) = R_H + S. \tag{9a}$$

Let R_H^* at a given frequency (f_1) be R_{H1}^*. Then, the R_H^* at a certain frequency (f_2), R_{H2}^* can be expressed as

$$R_{H2}^* = R_{H1}^* + dR_H^*, \tag{9b}$$

where dR_H^*, the differential increment, can be written by (9c).

$$dR_H^*(\text{dB}) = \frac{d}{df}(R_H + S)df. \tag{9c}$$

By substituting (7b) and (8) into (9c) and differentiating with respect to the frequency (f), dR_H^* can be derived as follows:

$$\begin{aligned} dR_H^* &= \frac{d}{df}\left[14.6 - 10\log\left(\frac{\mu_r}{fr^2\sigma_r}\right) + 20\log\left(\frac{c}{2fl}\right)\right]df \\ &= \left(\frac{10}{\ln 10}\frac{fr^2\sigma_r}{\mu_r}\frac{\mu_r}{f^2r^2\sigma_r} - \frac{20}{\ln 10}\frac{2fl}{c}\frac{c}{2f^2l}\right)df \\ &= \left(\frac{10}{f}\frac{1}{\ln 10} - \frac{20}{f}\frac{1}{\ln 10}\right)df = -\left(\frac{10}{f}\frac{1}{\ln 10}\right)df. \end{aligned} \tag{9d}$$

Notably, dR_H^* has a negative increment, indicating that the rate of increase of R_H is lower than the rate of decrease of S. Thus, R_H^* decreases gradually instead of increasing as frequency increases. dR_H^* can be calculated easily and directly from (9d). Given that the SE was measured at frequency intervals of ten from 10 kHz to 10 GHz, where df corresponded to $9f_1$ (f_2- f_1 = 10f_1 - f_1 = 9f_1); accordingly, dR_H^* results in -3.91 dB. This means that the SE of the sample with the small incident area decreased in the H-field by the corresponding incremental with the increase of the frequency by a factor of 10. A good agreement was observed between the derived result of -3.91 dB and the reduction rate of the experimental results. However, this tendency was not observed in the result for the large incident area samples. This is possibly because the aperture effect was removed by increasing the dimension of the incident area. S decreases with an increase in l, as indicated by (8).

The SE for a plane wave was hardly affected by the aperture effect. Note again that (8) can be used only when l is less than $\lambda/2$, and S decreases with the frequency. The l value of the small samples was 425 mm ($\sqrt{2}\times$ 300 mm) which is larger than 150 mm, corresponding to $\lambda/2$ at 1 GHz (the lowest experimental frequency in the plane wave region). Thus, (8) cannot be used for a plane wave. Specifically, the aperture effect decreased with increasing frequency, and it eventually disappeared in the plane wave region. Note that

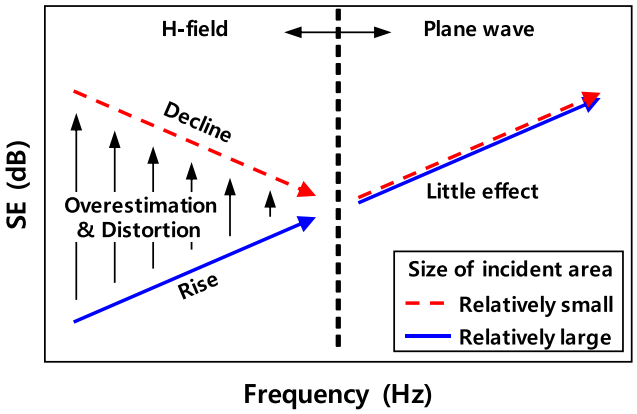

FIGURE 9. Effect of the incident area size on the EMI SE.

the SE values obtained for small and large incident areas were almost identical at above 1 GHz. This demonstrates that the effect of the aperture on SE for a plane wave was small regardless of the size of the incident area. However, if the SE test is performed using a sample with l smaller than 150 mm, the SE for a plane wave could be distorted owing to the aperture effect, but the effect is not significant.

In the case where the SE was measured for a large incident area, it temporarily decreased in the frequency range of 10–100 MHz, which is defined as the resonant and transition region. This is because resonance occurred in this region. Resonance occurs when $l = \lambda/2$. Given that the l value of the large incident area was approximately 1700 mm ($\sqrt{2}\times$ 1200 mm), the resonant frequency corresponding to $\lambda/2$ was calculated as 88 MHz. Thus, the resonance occurred at a resonant frequency of approximately 88 MHz, resulting in an SE reduction.

In summary (Fig. 9), the SE results for small and large incident areas are correlated with the frequency region. When testing the SE of UHPC/CNT composites according to IEEE-STD-299 in the H-field, samples should be fabricated to have an incident area of at least 1200 $\times$ 1200 mm^2 to eliminate the aperture effect. Otherwise, the SE could be overestimated and distorted. However, the SE for a plane wave is hardly affected by the aperture effect to be sufficient to represent the SE for the actual structure regardless of the size of the incident area. This finding can be applied to not only UHPC/CNT composites, but also cementitious materials such as cement paste, mortar, and concrete, because they have similar electrical resistivity.

3) PRACTICAL MODEL FOR ESTIMATING SE OF UHPC/CNT COMPOSITES

Equations (6) and (7) can be used to analyze the trend of the SE for a cementitious material without an aperture (e.g., with the increasing frequency, both A and R increase in the H-field, whereas for a plane wave, A increases and R decreases), but they cannot be used to calculate the SE. This is because the equations were derived for metals, which have good electrical properties, whereas cementitious materials have poor electrical properties. Thus, if the SE of the cementitious material is calculated using the previous equations, although the overall trend of the calculated SE can be similar to the experimental results, the accuracy is not guaranteed. For this reason, many researchers have attempted to develop a model to predict the SE of cementitious materials [28]–[31]. However, these previous models require information on variables that are difficult to measure such as μ_r, ε_r, and the moisture content to estimate SE. Therefore, they have limited use in practical situations.

Hence, a practical model to approximately estimate the SE of UHPC/CNT composites in terms of simple properties that are easy to measure, such as σ_r, r, t, and the frequency of interest f, is proposed according to the experimental results. The proposed model consists of equations for calculating the EMI SE in the H-field and for a plane wave, respectively, as follows:

$$\text{SE (dB)} = \begin{cases} 188.384\left(\dfrac{1}{fr^2\sigma_r}\right)^{-0.236} & \text{for H-field} \quad (10a) \\ \text{where } 10\text{ kHz} \le f \le 10\text{ MHz} & \\ \beta\sqrt{f} + 1.35 & \text{for plane wave} \quad (10b) \\ \text{where } \beta = \dfrac{\text{SE}_{1\text{GHz}} - 1.35}{\sqrt{10^9}}, \ 1\text{ GHz} < f \le 18\text{ GHz} & \end{cases}$$

To construct the model, it is first assumed that the μ_r and ε_r of the UHPC/CNT composites are 1 and 4.94, respectively [32], regardless of the CNT content. This assumption is made because the CNTs are not magnetic materials and cannot improve μ_r [33]. Moreover, a carbon filler, e.g., CNTs, can significantly affect the relative conductivity σ_r, whereas it has little effect on the relative permittivity ε_r [12], [28], [34], [35].

Initially, a regression model was employed to estimate the SE in the H-field according to the experimental results. In the H-field, R can be regarded as the SE because R is the key factor for determining the SE, and the contribution of A is negligible. Therefore, (7b) was revised as (10a) by performing regression analysis using the software SPSS Statistics 25.0. Fig. 10 shows the results of the regression analysis for R_H. The experimental data are scattered around the line plotted by the regression equation (10a). In Table 5, which is a summary of the regression analysis, the significance (Sig.) is less than 0.001. Accordingly, it is considered that there is a significant relationship between the independent variables (f, r^2, and σ_r) and the dependent variable (R_H) in the model. In addition, because the coefficient of determination (R^2) is 0.826, it can be considered that this model implies that there is an 82.6 % variability in the dependent variable. In statistics, a regression model in which R^2 is greater than 0.7, and a Sig. less than 0.001 is regarded as significant enough to be applied as an estimation model. Thus, (10a) can be applied to estimate the SE in the H-field.

When a plane wave passes through a material, its amplitude is attenuated exponentially as a function of the skin

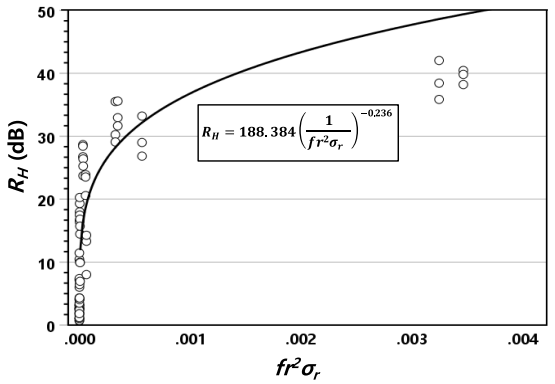

FIGURE 10. Results of the regression analysis for R_H.

TABLE 5. Summary of regression analysis for R_H.

Equation type	Model summary					Parameter estimates	
	R^2	F	Dof1	Dof2	Sig.	Constant	b1
Power	**0.826**	332.84	1	70	**0.000**	188.384	-0.236

depth (δ) [36]. The δ can be calculated as follows [27]:

$$\delta\,(\mathrm{m}) = \frac{0.066}{\sqrt{f\mu_r\sigma_r}}. \tag{11}$$

A can also be calculated by substituting (11) into (6).

Fig. 11 shows the δ of the UHPC/CNT composites and copper calculated using (11). The δ of the UHPC/CNT composites was very thick in the entire plane wave region, whereas that of the copper was very thin. However, as the CNT content increased, the δ of the UHPC/CNT composites decreased owing to the decrease in resistivity. Therefore, the UHPC/CNT composites cannot be regarded as a conductor as copper, but it can be regarded as lossy dielectric material, where the incident plane wave is partially reflected causing R, while the remainder penetrates and is attenuated resulting in A.

Hence, (10b) is derived using the following procedure. First, the impedance ratio (K) is calculated using (4) and (5) to determine the contribution of R to the SE for a plane wave (R_p). It is expressed as follows:

$$K = \frac{Z_m}{Z_w} = \sqrt{\left(\frac{\mu_o}{\varepsilon_o\varepsilon_r}\right) / \left(\frac{\mu_o}{\varepsilon_o}\right)} = \sqrt{\frac{1}{\varepsilon_r}}. \tag{12}$$

Then, R_P is calculated as 1.35 dB regardless of the frequency by substituting (12) into (7a). This indicates that for a plane wave, the contribution of R is very small, and the major factor determining the SE is A.

To derive the appropriate equation to calculate A for a plane wave, the experimental SE value measured at 1 GHz ($\mathrm{SE_{1GHz}}$) was used as the reference. Theoretically, a frequency corresponding to a plane wave starts at 28.09 MHz, but this frequency is within the resonant and transition region. Hence, it is not appropriate as the reference frequency to estimate SE

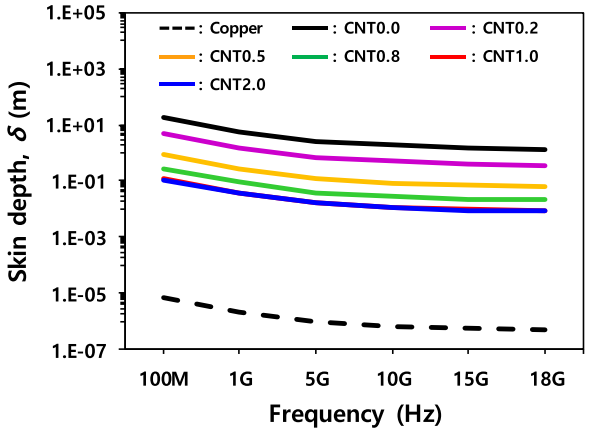

FIGURE 11. Skin depth (δ) of the specimens and copper.

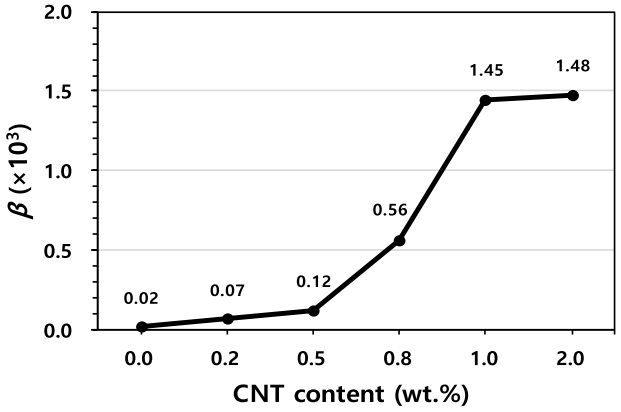

FIGURE 12. Calculated value of β with respect to the CNT content.

at high frequencies for a plane wave. In addition, because the δ of the samples calculated at 100 MHz (Fig. 11) was thicker than the thickness of the samples (0.2 m), it cannot be considered that sufficient A has been occurred at 100 MHz. However, the δ at 1 GHz was smaller than the thickness of the samples, except samples CNT0.0 and CNT0.2, where SE were close to 0 dB so that A can be considered to be occurred enough at 1 GHz. Thus, $\mathrm{SE_{1GHz}}$, i.e., the first measured SE value in the plane wave outside of the resonant and transition region, was selected as the reference. It is reasonable that an A at 1 GHz ($A_{1\mathrm{GHz}}$) can be calculated by subtracting R_P from $\mathrm{SE_{1GHz}}$. Then, $A_{1\mathrm{GHz}}$ is equated with (6) as follows:

$$A_{1\mathrm{GHz}} = SE_{1\mathrm{GHz}} - R_p = 131.4t\sqrt{f\mu_r\sigma_r}, \tag{13a}$$

Let $131.4t\sqrt{\mu_r\sigma_r}$ be equal to β. Then, the constant β is obtained as follows:

$$\beta = \frac{A_{1\,\mathrm{GHz}}}{\sqrt{f}} = \frac{\mathrm{SE_{1GHz}} - R_P}{\sqrt{10^9\,(1\,\mathrm{GHz})}}, \tag{13b}$$

β is directly calculated from (13b). The value increases with the CNT content owing to the improvement of the electrical conductivity, and the slope is similar to that of the reciprocal of the electrical resistivity (Fig. 4), as shown in Fig. 12.

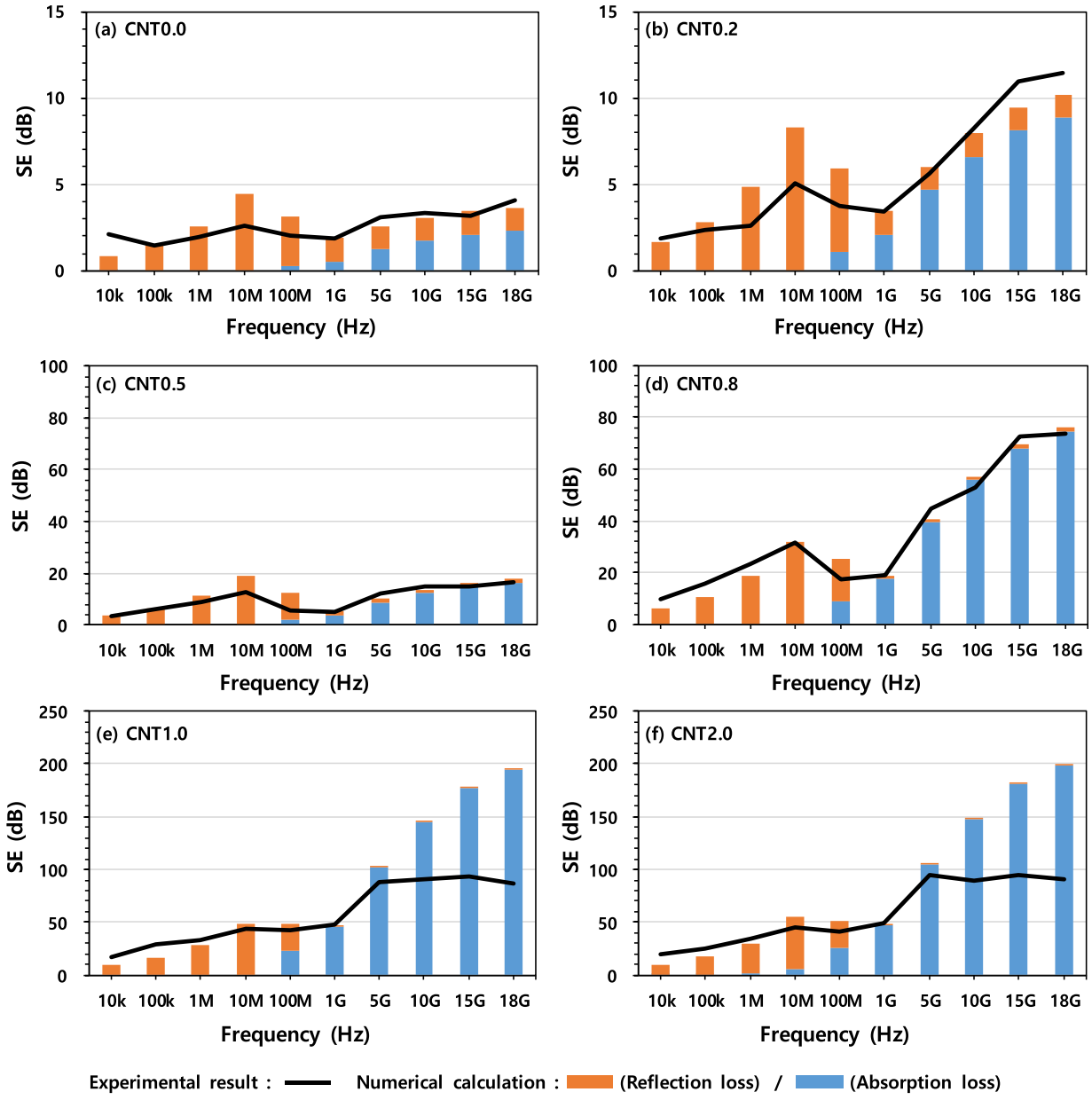

FIGURE 13. Comparison of the EMI SE results for the experimental data and numerical calculations using the proposed model.

Therefore, the A at other frequencies (A') can be expressed as follows:

$$A' = \beta\sqrt{f}. \tag{13c}$$

Consequently, the equation for estimating the SE for a plane wave can be derived as (10b) by combining (13c) with the calculated R_p value of 1.35.

The SE at frequencies between 10 MHz and 1 GHz can be calculated via a linear interpolation using the calculated SE value at 10 MHz and the experimental value of SE_{1GHz}.

To validate the suitability of the proposed model, the estimated SE results obtained by applying the preceding approach were compared with the experimental SE results. Specifically, the SE in the H-field was calculated by substituting the frequency of interest (10 kHz–10 MHz), sample-to-transmitting antenna distance (0.3 m), and relative conductivity of the samples calculated using the resistivity results (Fig. 4) into f, r, and σ_r in (10a). Then, the SE for a plane wave was calculated by substituting the β obtained from (13b) and the frequency of interest (1–18 GHz) into (10b). Subsequently, the SE in the resonant and transition region (10–100 MHz) were calculated via a linear interpolation. The comparison of the SE results between the experimental results and numerical calculation is shown in Fig. 13, indicating good

agreement. Most of the calculated SE is caused by R in the H-field and by A for a plane wave. It should be noticed again that this is because in the H-field, the δ is calculated as very thick, as indicated in (11), so the incident EM waves are not attenuated well (i.e., A hardly occurred), whereas R increases with the frequency, as indicated in (7b). However, for a plane wave, the δ decreases as frequency increases, so A increases, but R decreases as evident in (7c), and its contribution is small based on the result of calculation using (7a).

Every SE result measured at 100 MHz was smaller than the value obtained via numerical calculations by the proposed model. This is because the frequency was in the resonant and transition region, as previously mentioned. However, the measured SE values for samples CNT1.0 and CNT2.0 at above 1 GHz were lower than those obtained via the numerical calculations. This is possibly because the transmitted signal power used in the experiment was weak. If a sufficiently high-power signal could be used to measure the SE up to 200 dB, it is expected that the measured SE will be similar to that of the calculated SE.

In summary, the proposed model can be used to practically estimate the SE of a UHPC/CNT composite. The SE in the H-field with respect to the frequency of interest can be estimated by measuring only the values of r, t, and σ_r. In addition, using the experimental value of SE_{1GHz}, the SE of higher frequencies can be predicted without performing further experiments. Therefore, this can reduce the necessary amounts of labor, time, resources, etc. The proposed model can be employed to estimate the SE for most cementitious materials because their electrical resistivity range is within the database range of the model. However, it is necessary to accumulate data and to modify the equations continuously based on the results of additional experiments to establish more robust model.

IV. CONCLUSION

This study experimentally investigated the EMI SE of UHPC/ CNT composites for the first time according to IEEE-STD-299 as well as the effect of the incident area size on the SE. According to the experimental results and a statistical analysis, a practical model for the estimation of the SE of UHPC/CNT composites was proposed. The main conclusions are as follows:

i) Dispersed CNTs can significantly reduce the electrical resistivity of UHPC/CNT composites up to the percolation threshold owing to the formation of conductive pathway in the matrix. The electrical resistivity of the reference sample was 121173.33 Ω·m whereas that of sample CNT1.0 (with a CNT content of 1.0 wt.%) exhibited a significant improvement (4.78 Ω·m).

ii) The SE of a UHPC/CNT composite can be improved with an increase in the CNT content up to the percolation threshold for all frequency bands. This demonstrates the close correlation between the electrical resistivity (or conductivity) and the SE. The SE of sample CNT1.0 at 10 kHz and 1 GHz increased by factors of approximately 8 and 25, respectively, compared to that of the reference sample.

iii) When the SE of UHPC/CNT composites is tested, the SE in the H-field is probably overestimated and distorted owing to the effect of the aperture if a sample with a relatively small incident area is used. However, the SE for a plane wave is hardly affected by the size of the incident area. This observation can be used to update the existing guides of IEEE-STD-299.

iv) The proposed model by statistical analysis can be used to estimate the SE for cementitious materials, particularly UHPC/CNT composites. It is sufficiently practical to use onsite. However, to improve the accuracy of the model, more appropriate data should be collected via further experiments and analyses, including the effect of CNTs on the permittivity of the composites.

Future studies should focus on the minimum dimensions of the incident area for eliminating the aperture effect, a reliable SE test method using samples with small incident area, analyses of the SE for UHPC/CNT composites in terms of conductivity and permeability, as well as the accuracy of prediction models based on experimental data under various conditions.

ACKNOWLEDGMENT

The Institute of Engineering Research in Seoul National University provided research facilities for this work. The authors would like to thank Kumho Inc. for providing the CNTs and Mr. B.-H. Lee, CEO of Will Technology for supporting the EMI SE test.

REFERENCES

[1] D. D. L. Chung, "Electromagnetic interference shielding effectiveness of carbon materials," *Carbon*, vol. 39, no. 2, pp. 279–285, Feb. 2001.
[2] T. L. Thomas, P. D. Stolley, A. Stemhagen, E. T. H. Fontham, M. L. Bleecker, P. A. Stewart, and R. N. Hoover, "Brain tumor mortality risk among men with electrical and electronics jobs: A case-control study," *JNCI: J. Nat. Cancer Inst.*, vol. 79, no. 2, pp. 233–238, Aug. 1987.
[3] C. Beall, E. Delzell, P. Cole, and I. Brill, "Brain tumors among electronics industry workers," *Epidemiology*, vol. 7, no. 2, pp. 125–130, Mar. 1996.
[4] S. Szmigielski, "Cancer morbidity in subjects occupationally exposed to high frequency (radiofrequency and microwave) electromagnetic radiation," *Sci. Total Environ.*, vol. 180, no. 1, pp. 9–18, Feb. 1996.
[5] B. Han, L. Zhang, and J. Ou, *Smart and Multifunctional Concrete Toward Sustainable Infrastructures*. Singapore: Springer, 2017, pp. 247–259.
[6] D. D. L. Chung, *Carbon Composites: Composites With Carbon Fibers, Nanofibers, and Nanotubes*, 2nd ed. Oxford, U.K.: Butterworth-Heinemann, 2017, pp. 333–386.
[7] I. W. Nam, H. K. Lee, J. B. Sim, and S. M. Choi, "Electromagnetic characteristics of cement matrix materials with carbon nanotubes," *ACI Mater. J.*, vol. 109, no. 3, pp. 363–370, May 2012.
[8] S. Avanish Pratap, M. Monika, C. Amita, and S. K. Dhawan, "Graphene oxide/ferrofluid/cement composites for electromagnetic interference shielding application," *Nanotechnology*, vol. 22, no. 46, Oct. 2011, Art. no. 465701.
[9] A. P. Singh, B. K. Gupta, M. Mishra, A. Chandra, R. B. Mathur, and S. K. Dhawan, "Multiwalled carbon nanotube/cement composites with exceptional electromagnetic interference shielding properties," *Carbon*, vol. 56, pp. 86–96, May 2013.
[10] B. Wang, Z. Guo, Y. Han, and T. Zhang, "Electromagnetic wave absorbing properties of multi-walled carbon nanotube/cement composites," *Construct. Building Mater.*, vol. 46, pp. 98–103, Sep. 2013.

[11] J. M. Chiou, Q. Zheng, and D. D. L. Chung, "Electromagnetic interference shielding by carbon fibre reinforced cement," *Composites*, vol. 20, no. 4, pp. 379–381, Jul. 1989.
[12] D. Micheli, R. Pastore, A. Vricella, R. B. Morles, M. Marchetti, A. Delfini, F. Moglie, and V. M. Primiani, "Electromagnetic characterization and shielding effectiveness of concrete composite reinforced with carbon nanotubes in the mobile phones frequency band," *Mater. Sci. Eng., B*, vol. 188, pp. 119–129, Oct. 2014.
[13] *Standard Test Method for Measuring the Electromagnetic Shielding Effectiveness of Planar Materials*, Standard ASTM D4935-18, 2018.
[14] *Standard Test Method for Electromagnetic Shielding Effectiveness of Durable Rigid Wall Relocatable Structures*, ASTM E1851-15, 2015.
[15] *High-Altitude EMP Protection for Fixed Ground-Based Facilities*, document MIL-STD-188-125-1, 2005.
[16] *IEEE Standard Method for Measuring the Effectiveness of Electromagnetic Shielding Enclosures*, IEEE Standard 299, 2007.
[17] G. M. Kim, B. J. Yang, G. U. Ryu, and H. K. Lee, "The electrically conductive carbon nanotube (CNT)/cement composites for accelerated curing and thermal cracking reduction," *Compos. Struct.*, vol. 158, pp. 20–29, Dec. 2016.
[18] S. Vaidya and E. N. Allouche, "Strain sensing of carbon fiber reinforced geopolymer concrete," *Mater. Struct.*, vol. 44, no. 8, pp. 1467–1475, Oct. 2011.
[19] S. Wang, S. Wen, and D. D. L. Chung, "Resistance heating using electrically conductive cements," *Adv. Cement Res.*, vol. 16, no. 4, pp. 161–166, Oct. 2004.
[20] F. Reza, J. A. Yamamuro, and G. B. Batson, "Electrical resistance change in compact tension specimens of carbon fiber cement composites," *Cement Concrete Compos.*, vol. 26, no. 7, pp. 873–881, Oct. 2004.
[21] S. H. Lee, S. H. Kim, and D. Y. Yoo, "Hybrid effects of steel fiber and carbon nanotube on self-sensing capability of ultra-high-performance concrete," *Construct. Building Mater.*, vol. 185, pp. 530–544, Oct. 2018.
[22] L. S. Lerner, *Physics for Scientists and Engineers*, vol. 1. Burlington, MA, USA: Jones and Bartlett, 1996.
[23] F. J. Baeza, O. Galao, E. Zornoza, and P. Garcés, "Multifunctional cement composites strain and damage sensors applied on reinforced concrete (RC) structural elements," *Materials*, vol. 6, no. 3, pp. 841–855, Mar. 2013.
[24] D. D. L. Chung, "Self-heating structural materials," *Smart Mater. Struct.*, vol. 13, no. 3, pp. 562–565, Apr. 2004.
[25] R. Perez, *Handbook of Electromagnetic Compatibility*, 1st ed. San Diego, CA, USA: Academic, 1995, pp. 401–443.
[26] S. Loya and H. Khan, "Analysis of shielding effectiveness in the electric field and magnetic field and plane wave for infinite sheet metals," *Int. J. Electromagn. Appl.*, vol. 6, no. 2, pp. 31–41, Jun. 2016.
[27] H. W. Ott, *Electromagnetic Compatibility Engineering*. Hoboken, NJ, USA: Wiley, 2009, pp. 238–301.
[28] L. Sandrolini, U. Reggiani, and A. Ogunsola, "Modelling the electrical properties of concrete for shielding effectiveness prediction," *J. Phys. D, Appl. Phys.*, vol. 40, no. 17, pp. 366–372, Aug. 2007.
[29] T. Bourdi, J. E. Rhazi, F. Boone, and G. Ballivy, "Modelling dielectric-constant values of concrete: An aid to shielding effectiveness prediction and ground-penetrating radar wave technique interpretation," *J. Phys. D, Appl. Phys.*, vol. 45, no. 40, Sep. 2012, Art. no. 405401.
[30] P. Debye, *Polar Molecules*. New York, NY, USA: Chemical Catalog Co., 1929, p. 172.
[31] T. Bourdi, J. E. Rhazi, F. Boone, and G. Ballivy, "Application of Jonscher model for the characterization of the dielectric permittivity of concrete," *J. Phys. D, Appl. Phys.*, vol. 41, no. 20, Oct. 2008, Art. no. 205410.
[32] H. Xu, B. Li, S. Xu, and H. Feng, "The measurement of dielectric constant of the concrete using single-frequency CW radar," in *Proc. 1st Int. Conf. Intell. Netw. Intell. Syst.*, Nov. 2008, pp. 588–591.
[33] Y. Dai, M. Sun, C. Liu, and Z. Li, "Electromagnetic wave absorbing characteristics of carbon black cement-based composites," *Cement Concrete Compos.*, vol. 32, no. 7, pp. 508–513, Aug. 2010.
[34] S. K. Yee and M. Z. M. Jenu, "Shielding effectiveness of concrete with graphite fine powder in between 50 MHz to 400 MHz," in *Proc. Asia–Pacific Symp. Electromagn. Compat. (APEMC)*, May 2013, pp. 1–4.
[35] X. Zhang and W. Sun, "Microwave absorbing properties of double-layer cementitious composites containing Mn–Zn ferrite," *Cement Concrete Compos.*, vol. 32, no. 9, pp. 726–730, Oct. 2010.
[36] K. L. Kaiser, *Electromagnetic Compatibility Handbook*. New York, NY, USA: Taylor & Francis, 2004, pp. 21–23.

MYUNGJUN JUNG received the B.S. degree in civil engineering from Korea Military Academy, South Korea, in 2005, and the M.S. degree in architectural engineering from Seoul National University, South Korea, in 2011, where he is currently pursuing the Ph.D. degree. His research interest includes development of smart concrete with EMI/EMP Shielding capabilities.

YOUNG-SOON LEE received the B.S. degree in electronic engineering from Kyungpook National University, South Korea, in 1979, the M.S. degree in electronic engineering from the Korea Advanced Institute of Technology, South Korea, in 1981, and the Ph.D. degree in electronic engineering from Kyungpook National University, in 1996. Since 1981, he has been a Professor with the Kumoh National Institute of Technology, South Korea. His research interests include electromagnetic theory and scattering problem in antenna, waveguide discontinuities, aperture coupling, and microwave circuit.

SUNG-GUL HONG received the B.S. and M.S. degrees in architectural engineering from Seoul National University, South Korea, in 1981 and 1983, respectively, and the Ph.D. degree in architectural engineering from Lehigh University, USA, in 1994. Since 1996, he has been a Professor with Seoul National University. His research interests include multifunctional concrete with EMI shielding, self-sensing, and conductivity.